Title

In vivo hyperpolarization transfer in a clinical MRI scanner

Journal

Magnetic Resonance in Medicine, 80(2)

ISSN

0740-3194

Authors

von Morze, Cornelius

Reed, Galen D

Larson, Peder E

et al.

Publication Date

2018-08-01

DOI

10.1002/mrm.27154

Peer reviewed

HHS Public Access

Author manuscript

Magn Reson Med. Author manuscript; available in PMC 2019 August 01.

Published in final edited form as:

Magn Reson Med. 2018 August ; 80(2): 480–487. doi:10.1002/mrm.27154.

In vivo hyperpolarization transfer in a clinical MRI scanner

Cornelius von Morze, Ph.D.[1], **Galen D. Reed**[2], **Peder E. Larson**[1], **Daniele Mammoli**[1], **Albert P. Chen**[2], **James Tropp**[3], **Mark Van Criekinge**[1], **Michael A. Ohliger**[1], **John Kurhanewicz**[1], **Daniel B. Vigneron**[1], and **Matthew E. Merritt**[4]

[1]Department of Radiology and Biomedical Imaging, University of California, San Francisco

[2]GE Healthcare, Dallas, Texas

[3]Berkshire Magnetics, Berkeley, California

[4]Department of Biochemistry, University of Florida, Gainesville

Abstract

Purpose—The purpose of this study was to investigate the feasibility of *in vivo* ^{13}C->^{1}H hyperpolarization transfer, which has significant potential advantages for detecting the distribution and metabolism of hyperpolarized ^{13}C probes, in a clinical MRI scanner.

Methods—A standalone pulsed ^{13}C RF transmit channel was developed for operation in conjunction with the standard ^{1}H channel of a clinical 3T MRI scanner. Pulse sequences for ^{13}C power calibration and polarization transfer were programmed on the external hardware and integrated with a customized water-suppressed ^{1}H MRS acquisition running in parallel on the scanner. The newly developed RF system was tested in both phantom and *in vivo* polarization transfer experiments in $^{1}J_{CH}$-coupled systems: phantom experiments in thermally polarized and HP [2-^{13}C]glycerol, and ^{1}H detection of [2-^{13}C]lactate generated from HP [2-^{13}C]pyruvate in rat liver *in vivo*.

Results—Operation of the custom pulsed ^{13}C RF channel resulted in effective ^{13}C->^{1}H hyperpolarization transfer, as confirmed by the characteristic anti-phase appearance of ^{1}H-detected, $^{1}J_{CH}$-coupled doublets. In conjunction with a pulse sequence providing 190-fold water suppression *in vivo*, ^{1}H detection of HP [2-^{13}C]lactate generated *in vivo* was achieved in a rat liver slice.

Conclusion—The results show clear feasibility for effective ^{13}C->^{1}H hyperpolarization transfer in a clinical MRI scanner with customized heteronuclear RF system.

Keywords

dynamic nuclear polarization; pyruvate; lactate; INEPT

Corresponding author: Cornelius von Morze, Department of Radiology and Biomedical Imaging, University of California, San Francisco, 1700 Fourth Street, Byers Hall Suite 102, San Francisco, CA 94158, cornelius.vonmorze@ucsf.edu, Phone: 415-514-4455, Fax: 415-514-4451.

Introduction

Hyperpolarized (HP) ^{13}C MRI, based on the method of dissolution dynamic nuclear polarization (1,2), is currently undergoing translation into studies of human disease (3,4). Localized metabolic activity of injected HP ^{13}C probes can be tracked via ^{13}C MRI, by exploiting chemical shift differences among metabolites. Numerous technical investigations have focused on strategies for optimally sampling the spatial-spectral distribution of the transient HP ^{13}C magnetization (reviewed in (5)). While nearly all the prior *in vivo* work has focused on direct detection, shifting the hyperpolarization from ^{13}C nuclei to nearby ^{1}H spins offers significant potential advantages for detecting and imaging the *in vivo* distributions and metabolic transformations of HP ^{13}C probes. These include theoretically increased sensitivity of detection and reduced requirements on imaging gradient areas, both of which are due to the ~4x higher gyromagnetic ratio of ^{1}H vs. ^{13}C. Moreover, in this approach, specialized ^{13}C receiver coils and electronics are supplanted by standard ^{1}H equipment, which more readily attains body noise dominance at the higher readout frequency (6), and potentially simplifies HP ^{13}C MRI acquisition since ^{1}H coils are already tightly integrated with well-developed MRI acquisition methods including parallel imaging (7,8).

Building on prior work *in vitro* (9–12), initial preclinical studies have reported the feasibility of *in vivo* ^{13}C->^{1}H hyperpolarization transfer via the method of insensitive nuclei enhanced by polarization transfer (INEPT) (13–15). However, while such sequences are widely implemented on NMR spectrometers and preclinical MRI systems, clinical MRI systems are not generally configured for heteronuclear polarization transfer experiments. In this work, we have developed a supplementary standalone pulsed ^{13}C RF channel to operate simultaneously with ^{1}H spectroscopic acquisition on a clinical 3T MRI scanner, thus facilitating ^{13}C->^{1}H polarization transfer via a simplified reverse INEPT-type sequence. The newly developed clinical hardware/software framework was applied for ^{13}C->^{1}H hyperpolarization transfer in $^{1}J_{CH}$-coupled systems in both phantom and *in vivo* experiments: phantom ^{1}H MR experiments in thermally polarized and HP [2-^{13}C]glycerol, and ^{1}H detection of HP [2-^{13}C]lactate generated from HP [2-^{13}C]pyruvate by enzymatic transformation via LDH in normal rat liver *in vivo*.

Methods

Development of a supplementary pulsed ^{13}C RF transmit channel

A commercial standalone 3T ^{1}H decoupler (GE Healthcare, Waukesha, WI) (16) was extensively modified to instead operate in a pulsed mode at ^{13}C Larmor frequencies, while the standard system ^{1}H RF channel was utilized simultaneously for ^{1}H transmit/receive. The apparatus consisted of three main, rack-mounted components: a Herley model 3445 RF amplifier with 2kW pulsed peak power and frequency range 10–130MHz (Ultra Electronics Herley, Lancaster, PA), an Agilent model E4438C (option package 601) vector electronic signal generator (ESG) with frequency range of 250kHz–6GHz (Agilent Technologies, Santa Clara, CA), and a Windows PC equipped with an Agilent model 82357A universal serial bus (USB) / general purpose input output (GPIO) interface used for controlling the

ESG. The purpose of the USB/GPIO interface is to carry waveform instructions from the USB port of the PC to the GPIO port of the ESG.

Software provided by the vendor to control the ESG from the PC, based on the Agilent VEE programming environment, was bypassed by directly issuing commands over the USB/GPIO connection using a custom software interface programmed in Matlab (Mathworks, Natick, MA). Commands employed the syntax of Standard Commands for Programmable Instruments (SCPI), which is supported by the ESG. This custom software interface allowed arbitrary complex RF waveforms (i.e. the ^{13}C pulse sequence) to be loaded onto the ESG, at arbitrary carrier frequencies and power levels, and to be played with arbitrary timing delays with respect to a TTL trigger signal received from the MRI scanner. The TTL signal from the scanner exciter board goes high during signal readout, and was fed to an external trigger port of the ESG to trigger the ^{13}C pulse sequence at a specified delay after the start of the prior ^{1}H readout. The custom software that we have written to enable generation of external RF pulses on the Agilent ESG, timed with synchronization to a MRI scanner pulse sequence, is available for download from Matlab File Exchange at: https://www.mathworks.com/matlabcentral/fileexchange/65372-cvonmorze-external-rf-mri, which is linked to the corresponding source code repository on GitHub.

For ^{1}H decoupling (17), the amplifier operates in a CW mode without any RF blanking, with irradiation provided continuously at two separate power levels during readouts and the intervals between readouts (to facilitate NOE enhancement, although this is not generally useful for the case of HP studies). Two highly selective frequency filters, placed in series, ensure that application of ^{1}H decoupling power does not interfere with ^{13}C detection. These filters were uninstalled for the purpose of the pulsed MR experiments described in this study. Instead, the amplifier was configured for RF blanking during readout intervals, using the same readout trigger that was also used for timing the execution of the ^{13}C pulse sequence. Since as described the TTL signal precisely marks the readout intervals, blanking of the amplifier was achieved by simply feeding the TTL trigger signal to the blanking input on the amplifier (which is designed to blank when the input is high), in addition to the external trigger port of the ESG.

The external RF system architecture is illustrated in Figure 1. ^{13}C pulse power was delivered using low loss LMR-400 coaxial cabling from the output of the RF amplifier through a bulkhead connector panel located in the rear of the scanner room and into one of the two linear modes of the ^{13}C channel (i.e. the 0° ^{13}C port) of a dual-tuned ^{13}C/^{1}H volume quadrature transceiver coil (*i.d.*= 4cm, *l*= 8cm), whose quadrature ^{1}H channel was connected as usual to the 3T clinical MRI scanner. For calibration of the external ^{13}C pulse power, the resulting ^{13}C MR signal was detected via the other linear mode (i.e. the 90° ^{13}C port), which was connected to the 3T MRI scanner. While this scheme requires twice the transmit power in order to attain a given flip angle as compared to quadrature excitation, it facilitated ^{13}C detection for direct calibration of the external pulse power, while the standard excitation by the MR scanner system RF was temporarily deactivated in software. A manufacturer-supplied “white noise” pickup coil circuit, which deactivates the receivers in the event of detection of extraneous RF power, was temporarily disabled for the purpose of all

experiments involving externally supplied RF power. No attempt was made to synchronize RF phase between ^{1}H and ^{13}C channels.

^{13}C pulse sequences

Two ^{13}C RF pulse sequences were programmed in Matlab to run on the ESG. One served for ^{13}C pulse power calibration, and the other for ^{13}C->^{1}H polarization transfer. The power calibration sequence consisted of a single 500μs hard pulse. The polarization transfer sequence (Figure 2) consisted of two consecutive 500μs hard pulses with 90° RF phase shift, with pulse centers separated by 3.33ms, or ~$1/(2{}^{1}J_{CH})$=1/(300Hz) (13). In addition to RF blanking the amplifier during signal readout, the ESG was also blanked outside of the pulse sequence execution intervals (i.e. no carrier signal was detectable at the output of the ESG). Each sequence was triggered to execute just prior to signal readout on the subsequent TR interval on the MRI scanner, via a programmed delay following the scanner TTL signal marking the beginning of the first MR signal readout. For both sequences, the exact timing of the pulse sequence with respect to MR signal readout was verified by monitoring RF amplifier output and scanner TTL trigger signals on a Tektronix model TDS5034B oscilloscope (Tektronix, Beaverton, OR). For power calibration, a 1mL vial containing 6M aqueous [^{13}C]urea and 1% 500mM Gd-DTPA (v/v) was excited with TR=5s. The results were used to determine the 90° ^{13}C power level.

Product operator description of polarization transfer sequence

A product operator analysis of the applied pulse sequence considering a J-coupled, ^{1}H-^{13}C spin pair is straightforward and does not differ substantially from the original INEPT analysis (13). The initial $90°_{x}$ excitation pulse produces pure phase-I_{y} coherence, which then evolves under the scalar J-coupling. With the evolution delay set to $1/(2J_{CH})$ (3.33 ms), the I_{y} coherence is transformed into a bilinear coherence with an amplitude scaled by the gyromagnetic ratio of ^{13}C as well as the DNP enhancement (*Enh*):

$$Enh \cdot \gamma_C I_{C_z} \xrightarrow{I_{C_x}(90)} -Enh \cdot \gamma_C I_{C_y} \xrightarrow{\pi J \tau 2 I H_z C_z} -Enh \cdot \gamma_C 2 I_{H_z} I_{C_x} \quad (1)$$

After the hard $90°_{y}$ pulse on the ^{13}C channel, the anti-phase magnetization is restored to the Z-axis, where the subsequent ^{1}H shaped pulse produces a $H_{xy}C_{z}$ bilinear coherence that will be transformed into pure ^{1}H coherence after a further 1/(2J) evolution period. The phase of the transverse ^{1}H bilinear term can be modulated by switching the phase of the ^{1}H readout pulse. As the transverse ^{1}H coherence is generated initially from an anti-phase coherence, the enhanced signal will be an anti-phase doublet without phase correction. Since this a true polarization transfer, the enhancement of the ^{1}H signal intensity is scaled by $\gamma(^{13}C)/\gamma(^{1}H)$, i.e., a measured enhancement of 10000 for a ^{13}C detected experiment can only produce an enhancement of 2500 for ^{1}H after INEPT transfer. The sequence as implemented neglects the 180° pulses on both the ^{1}H and ^{13}C channels, as normally used, as both the ^{1}H and ^{13}C resonances were placed directly on resonance. Without the constraints of broadband polarization transfer, the sequence as implemented is considerably simpler than refocused

versions of INEPT. In our implementation, the slight temporal offset between the near-simultaneous ^{13}C and ^{1}H pulses does not change the analysis of the sequence significantly.

Water suppression sequence

Suppression of endogenous water signal is critical for ^{1}H detection of transferred hyperpolarization *in vivo*. To this end, a custom spectrally selective water suppression module (18) was programmed for the ^{1}H MRS sequence on the MRI scanner, which consisted of a train of ten consecutive 90° maximum phase Shinnar-LeRoux (SLR) pulses (19) with attendant spoiler gradient pulses. Although spectral selectivity was not required, the suppression sequence was adapted from a module that was originally designed for selective quenching of specific HP ^{13}C resonances (20) and therefore utilized spectrally selective RF pulses (pulse width= 13ms), centered on the water peak. For the in vivo experiments, this suppression train was executed at the beginning of each TR interval, just prior to ^{1}H excitation and detection. A delay of 8ms was appended to the end of the pulse train to allow a window for execution of the ^{13}C sequence before ^{1}H excitation / readout. The degree of water suppression that could practically be achieved using this sequence was measured *in vivo* in a normal rat.

MR experiments

To test the basic feasibility of ^{13}C->^{1}H hyperpolarization transfer using this custom setup, we first hyperpolarized 30μL [2-^{13}C]glycerol (Cambridge Isotopes, Tewksbury, MA), mixed with 15mM trityl radical OX063, in a commercial Hypersense dissolution DNP polarizer operating at 1.3K and 3.35T with ~94.1GHz microwave irradiation (Oxford Instruments, Tubney Woods, UK). Following buildup of hyperpolarization, the solid sample was rapidly dissolved in 5mL superheated D_2O to obtain a solution of 80mM HP [2-^{13}C]glycerol and transferred to the MRI scanner. ^{13}C hyperpolarization was transferred to the proton attached to the labeled carbon, using the described polarization transfer sequence running on the external hardware alongside the ^{1}H MR spectroscopy sequence running on the scanner. The sequence was executed twice with TR=1s, with the first readout triggering execution of the external ^{13}C 90°x-90°y sequence just prior to the second readout. On the ^{1}H side, excitation was by a single 500μs 90° hard pulse, with a subsequent readout of 2048 points and 5kHz sweep width. The ^{13}C sequence was completed about 200μs prior to the ^{1}H excitation pulse. We also repeated the same polarization transfer experiment using a vial phantom containing 3 grams of thermally polarized [2-^{13}C]glycerol.

Next, the potential for ^{1}H detection of [2-^{13}C]lactate generated from HP [2-^{13}C]pyruvate *in vivo* was tested in a normal Sprague Dawley rat. Animal experiments were conducted in accordance with a protocol approved by the Institutional Animal Care and Use Committee (IACUC). The rat was anesthetized using inhalational isoflurane (1.5%, 1L/min O_2 flow rate), with lateral tail vein catheter implanted prior to imaging. MR acquisition was identical to the phantom experiment except for two key differences: 1) The water suppression module was appended to the beginning of each TR of the pulse sequence, and 2) Instead of ^{1}H hard pulse excitation, an 8mm axial ^{1}H slice through the rat liver was excited with center frequency on water, using a slice selective 1.8ms windowed sinc pulse excitation. The ^{13}C sequence timing was adjusted so that it again completed about 200μs prior to the ^{1}H

excitation pulse. For the HP experiment, 24μL [2-^{13}C]pyruvic acid was hyperpolarized via DNP and subsequently dissolved in 4.6mL 80mM NaOH/Tris buffer. The resulting 80mM HP [2-^{13}C]pyruvate sample was injected over 12s, and the MR acquisition sequence was started 25s after the start of injection. To stimulate the exchange of the HP label into the lactate pool, an equimolar quantity of sodium lactate (natural abundance) was co-injected at the same time as the HP [2-^{13}C]pyruvate (21,22).

Results

Operation of the newly developed, external pulsed ^{13}C RF transmit system in conjunction with ^{1}H spectroscopic acquisition on the clinical scanner resulted in effective ^{13}C->^{1}H hyperpolarization transfer. Polarization transfer in the HP [2-^{13}C]glycerol phantom was evidenced by the characteristic anti-phase appearance of the resulting ^{1}H signal doublet on the second readout (Figure 3), following execution of the ^{13}C sequence. Initial ^{1}H hyperpolarization of this doublet (in-phase) was also observed on the first readout, an effect which is probably due to cross relaxation (23), but was largely extinguished by the first ^{1}H excitation. On the second TR, the signal-to-noise ratio (SNR) for each half of the detected signal doublet was in excess of 500:1. Because of the time required to transport the HP sample to the MRI scanner, the MR pulse sequence could not be started until 23s after the start of the dissolution. Since the ^{13}C T_1 relaxation time of [2-^{13}C]glycerol was separately measured to be ~7s in D_2O at 3T, we estimate that ~96% of the initial polarization was lost prior to MR data acquisition. Nevertheless, this experiment shows clear feasibility for polarization transfer via the described MRI system configuration. We also confirmed the efficacy of polarization transfer in the thermally polarized phantom containing [2-^{13}C]glycerol, noting an anti-phase shift in the intensities of the ^{13}C-coupled ^{1}H doublet (Figure 4). The effect is much more subtle in this case, when transferring only the tiny thermal polarization of ^{13}C, but very clear on the difference spectra.

Transfer of hyperpolarization was also evident in the *in vivo* rat experiment using HP [2-^{13}C]pyruvate. In this case, the hyperpolarization of [2-^{13}C]lactate generated enzymatically *in vivo* from HP [2-^{13}C]pyruvate via LDH was transferred to the directly bonded proton. In contrast to the phantom experiment, which was purposefully conducted in D_2O, water suppression was critical for the detection of polarization transfer *in vivo*. Application of the water suppression module resulted in 190-fold suppression of the endogenous water signal in the rat liver slice, based on comparing the area under the water peak with and without the suppression sequence. Slice selection for ^{1}H MRS resulted in much better water suppression as compared to non-selective mode (~20-fold increase), due to the greater B_1 homogeneity over the slice. Similar to the phantom results, a resonance corresponding to transferred HP lactate clearly appeared on the second ^{1}H MRS readout (Figure 5), following execution of the ^{13}C sequence. Despite effective water suppression, the other half of the ^{1}H lactate doublet could not be detected, probably because it was swamped by the large water peak.

Discussion

Our results extend into a clinical MRI scanner environment prior initial reports demonstrating the feasibility of *in vivo* ^{13}C->^{1}H hyperpolarization transfer (14,15). This functionality was enabled by developing an external pulsed ^{13}C RF transmit channel, for operation in conjunction with a water-suppressed, localized ^{1}H MRS acquisition sequence running in parallel on the scanner. An alternate, potentially easier, approach could be to modify the scanner system itself to support simultaneous multi-nuclear excitation, if it can support this mode. At least two prior studies have described scanner system changes along these lines. Gordon et al enabled simultaneous imaging of HP ^{13}C and ^{1}H nuclei on a 4.7T preclinical system (24). Wild et al re-engineered a 3T clinical scanner to support near-simultaneous imaging of three different nuclei (HP ^{3}He and ^{129}Xe, as well as ^{1}H) (25). Our study is the first to our knowledge to enable hyperpolarization transfer in a clinical system. The customized external RF system has potential advantages of increased flexibility and vendor neutrality. The key additional hardware required for our external approach is a vector RF ESG and RF amplifier. “Ballpark” cost estimates for these two components are: $20–30K for a new high-end RF ESG comparable to the model used in this study, and $25–50K for a RF amplifier with comparable output power and performance. Alternatively, a MRI system equipped with a secondary “broadband” amplifier dedicated to non-^{1}H studies could easily be modified for driving with an external ESG. Custom software is also required for this approach. We have successfully programmed one external ESG (Agilent) for the purpose of timed MRI pulse generation, and we are freely distributing the source code online.

In contrast to a recent study showing the feasibility of *in vivo* polarization transfer from HP [1-^{13}C]lactate (generated in vivo from [1-^{13}C]pyruvate) to its distant methyl protons (with J_{CH}=4.1Hz) (15), much larger couplings (~150Hz) characterize the $^{1}J_{CH}$ systems investigated in this work ([2-^{13}C]glycerol and [2-^{13}C]lactate). This case has the significant advantage of much shorter required evolution times, which go with $1/J_{CH}$, therefore minimizing the loss of polarization due to T_2 decay during the transfer process. Furthermore, the refocusing pulses necessary for standard INEPT acquisition are not required in this case, since $(1/J_{CH}) \ll T_2^*$. Another consideration when comparing the two systems is that the ^{13}C T_1 relaxation times of the $^{1}J_{CH}$-coupled species are also much shorter than [1-^{13}C]lactate as a result of larger dipolar coupling, which increases together with the larger J-coupling, potentially resulting in greater loss of polarization prior to transfer. This is not a fundamental limitation of our approach, however, as the lifetime of the HP metabolic product is much less important than its (relatively unaffected) precursor. In contrast to the HP precursor molecule, which is subject to a long delay period during transit and delivery to the target tissue of interest, the lifetime of the HP metabolic product need only be sufficiently long for its detection immediately after it is generated. Lastly, it is important to also note that a short additional delay would be required to match the in-phase condition for the transferred doublet, in conjunction with ^{13}C decoupling to collapse it to a singlet. For proof of principle, however, the anti-phase doublet provides valuable experimental proof for the efficacy of polarization transfer, in contrast with hyperpolarization of this proton via cross-relaxation (23).

While the described water suppression scheme was sufficiently effective (providing 190-fold suppression) to facilitate detection of transferred HP ^{1}H lactate signal, the other half of the signal doublet could not be detected, probably due to residual interference from water signal. For this initial work we have adopted a relatively basic water suppression scheme consisting of a 90° pulse train. Future work will focus on improving the effectiveness of water suppression, likely utilizing a combination of RF and gradient-enhanced approaches. We anticipate that a high degree of suppression should be feasible by application of coherence selection gradients (26). The basic principle of this approach is to apply different gradient areas to the transverse magnetization before and after polarization transfer, according to the difference in gyromagnetic ratios between the two nuclei. In this manner, gradients are balanced only for transferred magnetization, resulting in near ideal suppression of background signal. Lipid suppression may also be important for some transfer targets, for example the methyl group protons in [1-^{13}C]lactate. In future studies, we will also aim to investigate the potential dynamic ^{1}H imaging of hyperpolarization transferred from ^{13}C, by implementing spectrally selective pulses on the external hardware with flip angles under 90°, so as to efficiently sample the magnetization dynamically.

References

1. Ardenkjaer-Larsen JH, Fridlund B, Gram A, Hansson G, Hansson L, Lerche MH, Servin R, Thaning M, Golman K. Increase in signal-to-noise ratio of > 10,000 times in liquid-state NMR. Proc Natl Acad Sci US A. 2003; 100:10158–10163. DOI: 10.1073/pnas.1733835100
2. Ardenkjaer-Larsen JH, Leach AM, Clarke N, Urbahn J, Anderson D, Skloss TW. Dynamic nuclear polarization polarizer for sterile use intent Rizi R, editor. NMR in Biomedicine. 2011; 24:927–932. DOI: 10.1002/nbm.1682 [PubMed: 21416540]
3. Nelson SJ, Kurhanewicz J, Vigneron DB, et al. Metabolic Imaging of Patients with Prostate Cancer Using Hyperpolarized [1-C-13]Pyruvate. Sci Transl Med. 2013; :5.doi: 10.1126/scitranslmed.3006070
4. Cunningham CH, Lau JY, Chen AP, Geraghty BJ, Perks WJ, Roifman I, Wright GA, Connelly KA. Hyperpolarized 13C Metabolic MRI of the Human Heart: Initial Experience. Circ Res. 2016; CIRCRESAHA.116.309769. doi: 10.1161/CIRCRESAHA.116.309769
5. Cho A, Lau JYC, Geraghty BJ, Cunningham CH, Keshari KR. Noninvasive Interrogation of Cancer Metabolism with Hyperpolarized (13)C MRI. J Nucl Med. 2017; 58:1201–1206. DOI: 10.2967/jnumed.116.182170 [PubMed: 28596156]
6. Edelstein WA, Glover GH, Hardy CJ, Redington RW. The intrinsic signal-to-noise ratio in NMR imaging. Magn Reson Med. 1986; 3:604–618. [PubMed: 3747821]
7. Sodickson DK, Manning WJ. Simultaneous acquisition of spatial harmonics (SMASH): fast imaging with radiofrequency coil arrays. Magn Reson Med. 1997; 38:591–603. [PubMed: 9324327]
8. Sodickson DK, Manning WJ. Simultaneous acquisition of spatial harmonics (SMASH): fast imaging with radiofrequency coil arrays. Magn Reson Med. 1997; 38:591–603. [PubMed: 9324327]
9. Frydman L, Blazina D. Ultrafast two-dimensional nuclear magnetic resonance spectroscopy of hyperpolarized solutions. Nat Phys. 2007; 3:415–419. DOI: 10.1038/nphys597
10. Sarkar R, Comment A, Vasos PR, Jannin S, Gruetter R, Bodenhausen G, Hall H, Kirik D, Denisov VP. Proton NMR of 15N-Choline Metabolites Enhanced by Dynamic Nuclear Polarization. J Am Chem Soc. 2009; 131:16014–16015. DOI: 10.1021/ja9021304 [PubMed: 19848401]
11. Chekmenev EY, Norton VA, Weitekamp DP, Bhattacharya P. Hyperpolarized 1H NMR Employing Low γ Nucleus for Spin Polarization Storage. J Am Chem Soc. 2009; 131:3164–3165. DOI: 10.1021/ja809634u [PubMed: 19256566]
12. Dzien P, Fages A, Jona G, Brindle KM, Schwaiger M, Frydman L. Following Metabolism in Living Microorganisms by Hyperpolarized 1H NMR. J Am Chem Soc. 2016; 138:12278–12286. DOI: 10.1021/jacs.6b07483 [PubMed: 27556338]

13. Morris GA, Freeman R. Enhancement of nuclear magnetic resonance signals by polarization transfer. J Am Chem Soc. 1979; 101(3):760–762. DOI: 10.1021/ja00497a058

14. Mishkovsky M, Cheng T, Comment A, Gruetter R. Localized in vivo hyperpolarization transfer sequences. Magn Reson Med. 2012; 68:349–352. DOI: 10.1002/mrm.23231 [PubMed: 22190079]

15. Wang J, Kreis F, Wright AJ, Hesketh RL, Levitt MH, Brindle KM. Dynamic (1) H imaging of hyperpolarized [1-(13) C]lactate in vivo using a reverse INEPT experiment. Magn Reson Med. 2017; 137:6418.doi: 10.1002/mrm.26725

16. Chen AP, Tropp J, Hurd RE, Van Criekinge M, Carvajal LG, Xu D, Kurhanewicz J, Vigneron DB. In vivo hyperpolarized 13C MR spectroscopic imaging with 1H decoupling. J Magn Reson. 2009; 197:100–106. DOI: 10.1016/j.jmr.2008.12.004 [PubMed: 19112035]

17. de Graaf, RA., Rothman, DL., Behar, KL. State of the art direct C-13 and indirect H-1-[C-13] NMR spectroscopy in vivo. A practical guide. In: Rizi, R., editor. NMR in Biomedicine. Vol. 24. 2011. p. 958-972.

18. Haase A, Frahm J, Hanicke W, Matthaei D. 1H NMR chemical shift selective (CHESS) imaging. Phys Med Biol. 1985; 30:341–344. DOI: 10.1088/0031-9155/30/4/008 [PubMed: 4001160]

19. Pauly J, Le Roux P, Nishimura D, Macovski A. Parameter relations for the Shinnar-Le Roux selective excitation pulse design algorithm [NMR imaging]. IEEE Trans Med Imaging. 1991; 10:53–65. DOI: 10.1109/42.75611 [PubMed: 18222800]

20. von Morze C, Chang G-Y, Larson PEZ, et al. Detection of localized changes in the metabolism of hyperpolarized gluconeogenic precursors (13) C-lactate and (13) C-pyruvate in kidney and liver. Magn Reson Med. 2016; doi: 10.1002/mrm.26245

21. Day SE, Kettunen MI, Gallagher FA, Hu D-E, Lerche M, Wolber J, Golman K, Ardenkjaer-Larsen JH, Brindle KM. Detecting tumor response to treatment using hyperpolarized 13C magnetic resonance imaging and spectroscopy. Nat Med. 2007; 13:1382–1387. DOI: 10.1038/nm1650 [PubMed: 17965722]

22. Hurd RE, Spielman D, Josan S, Yen Y-F, Pfefferbaum A, Mayer D. Exchange-linked dissolution agents in dissolution-DNP (13)C metabolic imaging. Magn Reson Med. 2013; 70:936–942. DOI: 10.1002/mrm.24544 [PubMed: 23165935]

23. Merritt ME, Harrison C, Mander W, Malloy CR, Sherry AD. Dipolar cross-relaxation modulates signal amplitudes in the (1)H NMR spectrum of hyperpolarized [(13)C]formate. J Magn Reson. 2007; 189:280–285. DOI: 10.1016/j.jmr.2007.09.011 [PubMed: 17945520]

24. Gordon JW, Fain SB, Niles DJ, Ludwig KD, Johnson KM, Peterson ET. Simultaneous imaging of 13C metabolism and 1H structure: technical considerations and potential applications. NMR in Biomedicine. 2015; 28:576–582. DOI: 10.1002/nbm.3279 [PubMed: 25810146]

25. Wild JM, Marshall H, Xu X, Norquay G, Parnell SR, Clemence M, Griffiths PD, Parra-Robles J. Simultaneous imaging of lung structure and function with triple-nuclear hybrid MR imaging. Radiology. 2013; 267:251–255. DOI: 10.1148/radiol.12121153 [PubMed: 23264344]

26. Ruiz-Cabello J, Vuister GW, Moonen CTW, van Gelderen P, Cohen JS, van Zijl PCM. Gradient-enhanced heteronuclear correlation spectroscopy: Theory and experimental aspects. Journal of Magnetic Resonance. 2011; 213:446–466. [PubMed: 22152362]

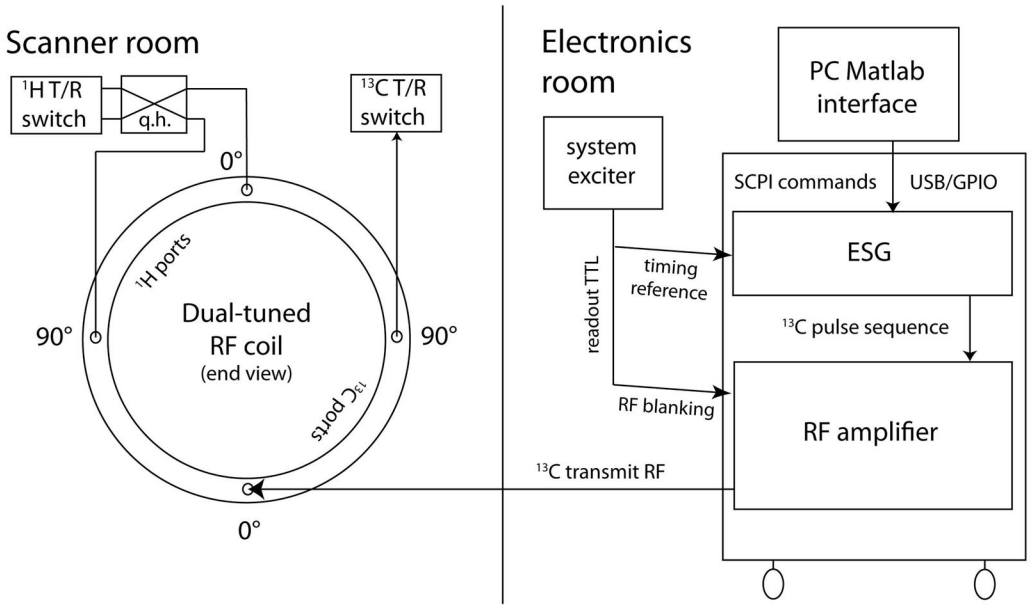

Figure 1.

System diagram for operation of supplementary ^{13}C RF transmit channel in conjunction with ^{1}H MRS on the clinical MRI scanner. The ^{13}C pulse sequence is executed on the independent ESG, which is programmed from a PC interface and timed with respect to a TTL signal from the system exciter board. Following amplification, ^{13}C transmit RF power is coupled into one of the two linear modes of the quadrature ^{13}C channel of a dual-tuned volume coil, while the other mode is coupled to the scanner ^{13}C receiver for the purpose of power calibration. The coil ^{1}H channel is connected to the ^{1}H transmit/receive (T/R) switch as usual through a quadrature hybrid (q.h.).

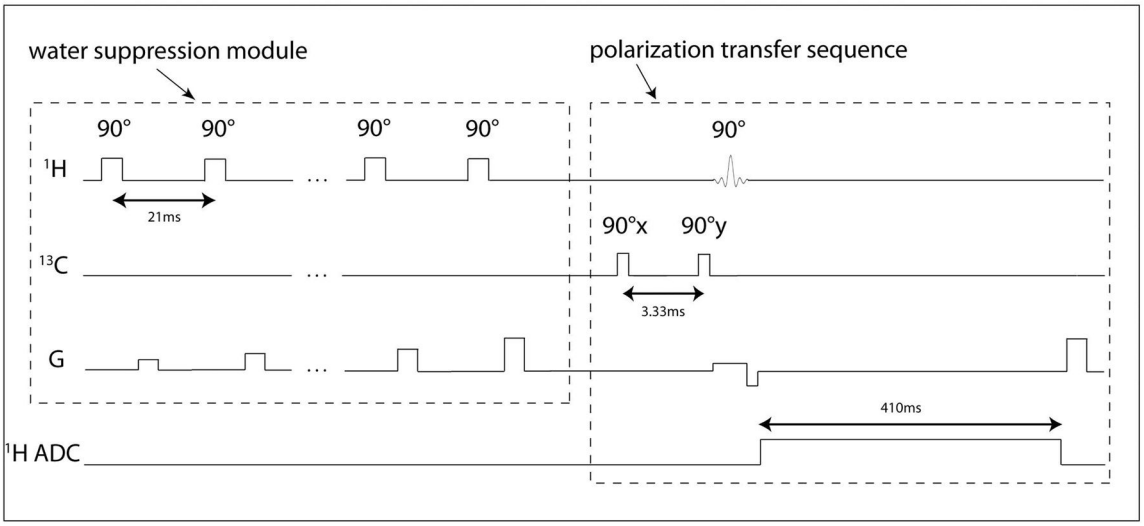

Figure 2.

Pulse sequence diagram for ^{13}C->^{1}H hyperpolarization transfer *in vivo*. The sequence is composed of a three-pulse, simplified INEPT-type polarization transfer sequence (right dotted box), preceeded by a water suppression module (left dotted box), consisting of ten consecutive 90° RF pulses with attendant spoiler gradients. ^{1}H transmit/receive utilized the standard system RF channel, while ^{13}C RF power was supplied by the external system.

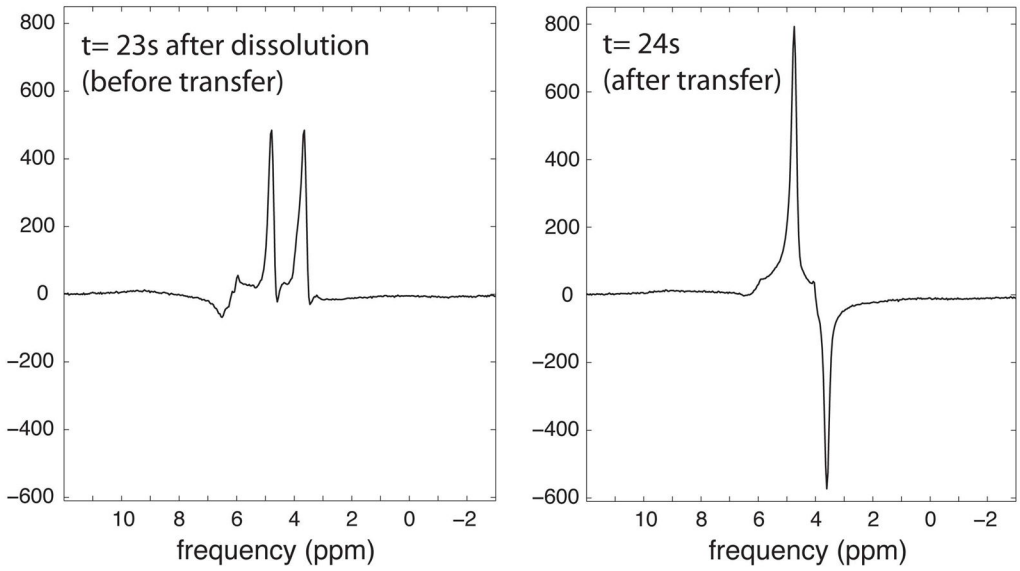

Figure 3.

Phased ^{1}H MR spectra (real) of HP [2-^{13}C]glycerol phantom collected on first (left) and second (right) TR intervals of the described polarization transfer sequence. The second spectrum clearly showed an anti-phase appearance characteristic of polarization transfer as described. The y-axes are scaled to units of approximate SNR.

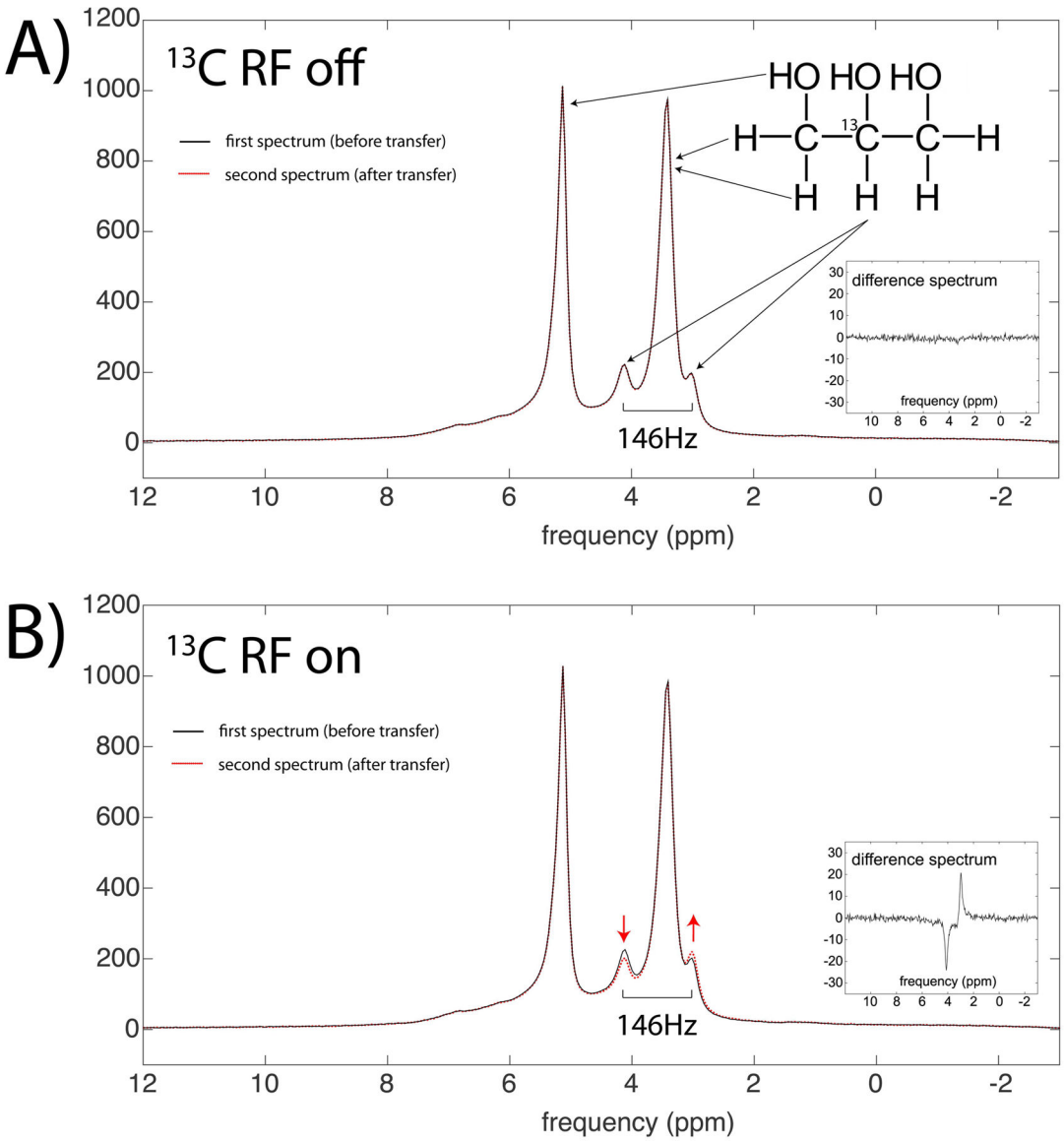

Figure 4.

Phased ^{1}H MR spectra (real) of thermally polarized [2-^{13}C]glycerol vial phantom. A subtle anti-phase shift in the intensities of the ^{13}C-coupled ^{1}H doublet is observed when the polarization transfer sequence is executed (B), but not when the external ^{13}C RF is deactivated (A). A pair of red arrows highlight the directionality of the shift. In each case, spectra acquired before (solid black line) and after (red dotted line) the transfer sequence are shown superimposed on a single axis. Difference spectra are shown as insets.

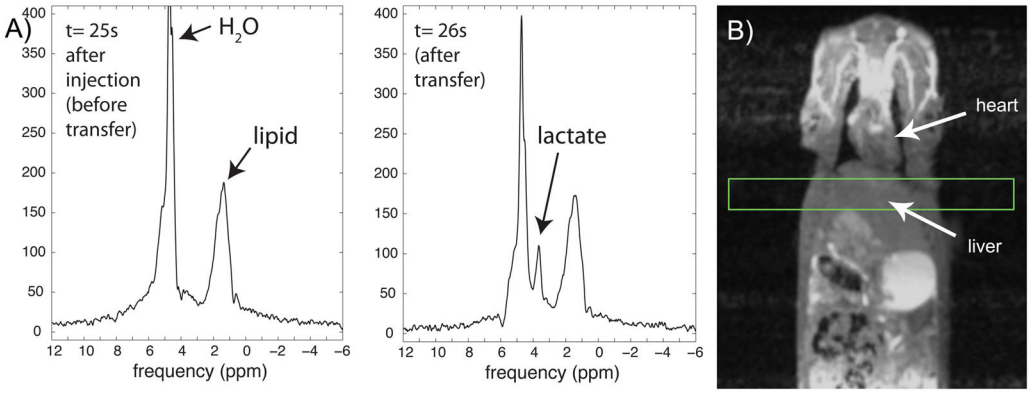

Figure 5.

In vivo localized ^{1}H detection of HP [2-^{13}C]lactate generated from [2-^{13}C]pyruvate in an 8mm axial slice through rat liver (A). The ^{1}H lactate peak appeared after the polarization transfer sequence was executed during the second TR interval (right panel of A). Magnitude spectra are shown. Position of the axial slice is shown in (B), overlaid on a coronal anatomic ^{1}H MRI image.